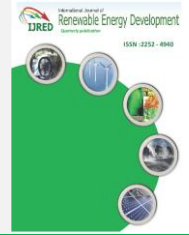




Contents list available at IJRED website

International Journal of Renewable Energy Development

Journal homepage: <https://ijred.undip.ac.id>



Research Article

Performance evaluation of the novel 3D-printed aquatic plant-microbial fuel cell assembly with *Eichhornia crassipes*

Mel Patrick D. Malinis^a, Herna Jones F. Velasco^a, Kristopher Ray S. Pamintuan^{a,b*}

^aSchool of Chemical, Biological, and Materials Engineering and Sciences, Mapua University, Manila, Philippines

^bCenter for Renewable Bioenergy Research, Mapua University, Manila, Philippines

Abstract. Plant-Microbial Fuel Cells (PMFCs) are a sustainable derivative of fuel cells that capitalizes on plant rhizodeposition to generate bioelectricity. In this study, the performance of the novel 3D-printed aquatic PMFC assembly with *Eichhornia crassipes* as the model plant was investigated. The design made use of 1.75 mm Protopasta Conductive Polylactic Acid (PLA) for the electrodes and 1.75 mm CCTREE Polyethylene Terephthalate Glycol (PETG) filaments for the separator. Three systems were prepared with three replicates each: PMFCs with the original design dimensions (System A), PMFCs with cathode-limited surface area variations (System B), and PMFCs with anode-limited surface area variations (System C). The maximum power density obtained by design was $82.54 \mu\text{W}/\text{m}^2$, while the average for each system is $26.99 \mu\text{W}/\text{m}^2$, $36.24 \mu\text{W}/\text{m}^2$, and $6.81 \mu\text{W}/\text{m}^2$, respectively. The effect of variations on electrode surface area ratio was also examined, and the results suggest that the design benefits from increasing the cathode surface area up to a cathode-anode surface area ratio of 2:1. This suggests that the cathode is the crucial component for this design due to it facilitating the rate-limiting step. Plant health was also found to be a contributing factor to PMFC performance, thereby suggesting that PMFCs are an interplay of several factors not limited to electrode surface area alone. The performance of the novel PMFC did not achieve those obtained from existing studies. Nevertheless, the result of this study indicates that 3D-printing technology is a possible retrofit for PMFC technology and can be utilized for scale-up and power amplification.

Keywords: 3D-printing, aquatic PMFC, performance evaluation, electrodes, electrochemistry



@ The author(s). Published by CBIORE. This is an open access article under the CC BY-SA license (<http://creativecommons.org/licenses/by-sa/4.0/>).

Received: 26TH March 2023; Revised: 21st July 2023; Accepted: 8th August 2023; Available online: 29th August 2023

1. Introduction

The continued energy demand driven by the continuously growing population and living standards has led to the reliance on non-renewable sources. Consequently, the emissions (particularly in the form of greenhouse gases) associated with its consumption ultimately led to irreversible impacts on the environment (Krishnan *et al.*, 2021). As such, renewable energy technologies that are simple and cost-effective should be capitalized on. An example of which is the Plant-Microbial Fuel Cell (PMFC). In its simplest sense, PMFCs are makeshift batteries whose fuel is the organic matter deposits on the roots of plants (Dave *et al.*, 2020). These organic deposits, termed rhizodeposit, are consumed by electrogenic bacteria (EAB) present in the rhizosphere, which then gives free electrons in the process. PMFCs make use of these free electrons by capturing them through their polarized electrode configuration, ultimately generating electricity in the process plants (Garbini *et al.*, 2023; Pamintuan, Ancheta, *et al.*, 2020; Roy *et al.*, 2023).

Over the course of years, progressions on PMFC mainly focused on its major challenge, low bioelectricity generation. Its weaknesses have been overcome by coupling it with other technologies, most of which are in the wastewater treatment regime (Kabutey *et al.*, 2019). Despite the limitations, the prospects of the PMFC technology had been capitalized by researchers to exploit its diverse capabilities. It has played with

various aspects from variations on electrode materials, techniques, and configurations, and on plant selection. In a study of Helder *et al.*, three different plants namely *Spartina anglica*, *Arundinella anomala* and *Arundo donax* were tested and compared for bio-electricity production and maximization of power output (Helder *et al.*, 2010). From these, *Spartina anglica* obtained the highest power density of all having $222 \text{ mW}/\text{m}^2$, outperforming the highest power density previously reported, specifically by Strik *et al.* and Timmers *et al.* which obtained $67 \text{ mW}/\text{m}^2$ and $100 \text{ mW}/\text{m}^2$ respectively (Strik *et al.*, 2008; Timmers *et al.*, 2010). While other studies such of Reyes *et al.* focused on optimizing the different electrode spacing, combinations and number through compartmentalization and polarization studies (Pamintuan, Reyes, *et al.*, 2020).

Although promising, PMFCs still have some issues they should address, which makes this field an active area for research. The major bottleneck for this technology is the small power density that can be harvested for a single cell. This has been addressed by stacking efficiency studies which amplify the power generated by PMFC systems by electrically connecting the cells in series and parallel (Pamintuan, Ancheta, *et al.*, 2020). Another is optimization studies, which sought to improve its performance through variations in electrode surface areas and other design aspects (Sharma & Chhabra, 2021). The electrode material is also a variable of focus, to which graphite and other carbon-derived materials are common due to it being

* Correspondence author

Email: krsbamintuan@mapua.edu.ph (K.R.S. Pamintuan)

inexpensive yet highly conductive. However, other possible electrode materials and technologies are still untapped – one of which is additive manufacturing. Recent studies have already employed this technology in the development of biological electrical systems. In the study of Theodosiou et al., MFCs with 3D-printed membrane electrode assemblies outperformed those with cation exchange membrane material in terms of power generation and cost-effectiveness (Theodosiou *et al.*, 2019). Another attempt at using 3D-printing technology was made by Halpenny, in which a fully 3D-printed PMFC using bryophytes was fabricated instead of a vascular plant (Halpenny, 2021). These attempts suggest that with properly engineered design, PMFCs can be easily reproduced and thereby expedite stacking, optimization, and other studies for improving PMFC performance. However, the majority of the studies available in the literature focus on integrating this technology on terrestrial PMFCs alone, and its use on aquatic systems are yet to be explored. Theoretically, power generation on the latter should be higher due to the lack of resistance on liquid media. As such, there is a need to investigate the applicability of 3D-printing technology on aquatic PMFCs.

In this study, a novel 3D-printed aquatic PMFC that is easy to operate and maintain was developed. The design utilized conductive filament as electrodes instead of conventional materials. It features a clip-like mechanism that makes it easy to install, thereby making onsite power generation possible. Moreover, the rapid prototyping advantage of 3D-printing technology provides further design improvements such as additional design retrofit and power amplification, thus making the novel design flexible to different studies of focus. The design was developed with *Eichhornia crassipes* as the model plant and its performance was evaluated. Its power generation was compared to those of the existing studies, and the effect of electrode surface area and other factors on its performance was also investigated. The results provided in this study can be a step for further design improvements and alternatives for existing crude assemblies. Also, the design will make use of an otherwise invasive species, thereby using its drawback to its advantage to deliver sustainable, cheap, and appreciable electricity.

2. Materials and Methods

2.1 Plant Microbial Fuel Cell Assembly

E. crassipes sourced from a lake in Taguig, Philippines, was utilized as the model free-floating macrophyte for the systems. The plants selected were of comparable sizes and were acclimatized continuously in 68-liter water basins with dechlorinated tap water substrate under partial shading. Acclimatization was performed until plants developed white roots to remain healthy. Afterward, PMFCs were clipped into the roots, as illustrated in Figure 1.

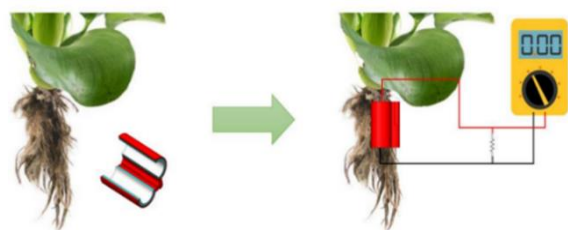


Fig 1. Individual PMFC Set Up

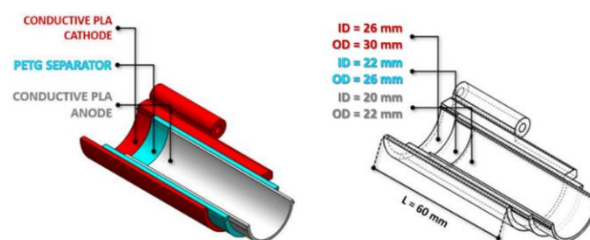


Fig 2. Aquatic PMFC components and dimensions

The assembly of the aquatic PMFC is composed of three components: the anode, separator, and cathode. The cathode facilitates the reduction reaction for the electrochemical reaction, while the oxidation reaction occurs in the anode. A separator was also utilized to serve as a physical boundary for the electrodes, which could otherwise result in an internal short circuit (Tornheim & O'Hanlon, 2020). Contrary to the conventional PMFC design, the electrode configuration in aquatic PMFCs is reversed, which the anode being the internal electrode. 1.75 mm Protopasta Conductive Polylactic Acid (PLA) and CCTREE Polyethylene Terephthalate Glycol (PETG) filaments were used for the electrodes and separator, respectively.

The design of the 3D-printed aquatic PMFC is analogous to that of a laundry clip. For this assembly, both cathode compartments are to be secured by a 3.2 mm diameter 3D-printed pin with the same filament as the electrodes. For the voltage and current measurements, the external circuit connections are established by clipping the alligator clips on the anode and cathode surfaces.

Three PMFC systems, labeled A, B, and C, were developed with three replicates each: PMFCs with the original design dimensions (System A), PMFCs with cathode-limited surface area variations (System B), and PMFCs with anode-limited surface area variations (System C). The schematic figures of system A, B, and C are illustrated in Figure 3. A summary of systems and their corresponding parameters to be observed is provided in Table 1.

The variations on the electrode surface area are conducted by adding ridges on the electrodes' exposed surface. This ensures that the design's structural integrity and filament consumption are not compromised and the internal resistance due to filament is not increased. Each cell was placed adjacent to each other, surrounding an MB-102 Solderless Breadboard (400 holes, 5.5 cm × 8.3 cm dimension) to which the external resistors were connected to avoid dangling wires in the setup.

For System B with anode-limited variation, round ridges of 1.5 mm radius were added on each of the cathode surfaces, resulting in an overall addition of 2, 6, and 10 ridges, whereas rectangular ridges of 60 mm × 1 mm × 5 mm dimensions were

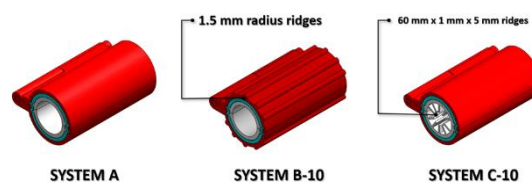


Fig 3. PMFC System A, B-10, and C-10 Schematic Diagram

Table 1
PMFC Systems to be studied.

System	Description	Parameters to be observed
A	3D-printed PMFC only	Power density
B	3D-printed PMFC with anode-limited variation	Power density; electrode surface area ratio
C	3D-printed PMFC with cathode-limited variation	Power density; electrode surface area ratio

Table 2
Calculated nominal surface areas of the exposed parts of the electrodes using Solidworks.

System	Number of ridges	Anode surface area, mm ²	Cathode surface area, mm ²	C/A Ratio
A	None (control)	3,954	7,409	1.87
	2	3,954	7,610	1.92
B	6	3,954	8,085	2.05
	10	3,954	8,525	2.16
	2	5,171	7,409	1.43
C	6	7,604	7,409	0.97
	10	8,847	7,409	0.84

added on the anode surface for System C. Likewise, the ridges are added vertically to prevent potential overhangs. Illustrations and dimensions of the PMFC systems are provided in Figure 4 and Table 2.

2.2 Measurement and Monitoring

The voltage and current readings were manually recorded four times daily (8 AM, 12 PM, 4 PM, 8 PM) for 14 days, followed by 7 days of single measurement using an Ingco Digital Multimeter. For voltage and current measurement, a parallel and series circuit configuration was utilized. The overall measurement was performed by connecting the PMFCs' jumper cable pins and alligator clips to the breadboard to which the multimeter will be connected. The voltage readings were acquired to serve as evidence that the PMFC is functioning effectively and as a basis to quantify the power generation from the microbial activity in the roots of the plant. Also, the resistances of the 3D-printed PMFCs were measured to determine the average resistivities of the anode and cathode. Afterwards, a preliminary polarization test was performed and was accomplished using resistors with values ranging from 100 Ω to 430,000 Ω in the voltage measurement configuration. From these values, power is calculated and plotted against the current to generate the Polarization curve, which determines the ideal resistor value for each system throughout the experiment. This is followed by a final polarization test after the experiment to determine the maximum power densities of each system. Power and power densities will be calculated from the obtained voltage and current readings. Finally, additional voltage measurements were held by swapping the plants of the best performing and least performing PMFCs to determine the significance of plant health to PMFC performance.

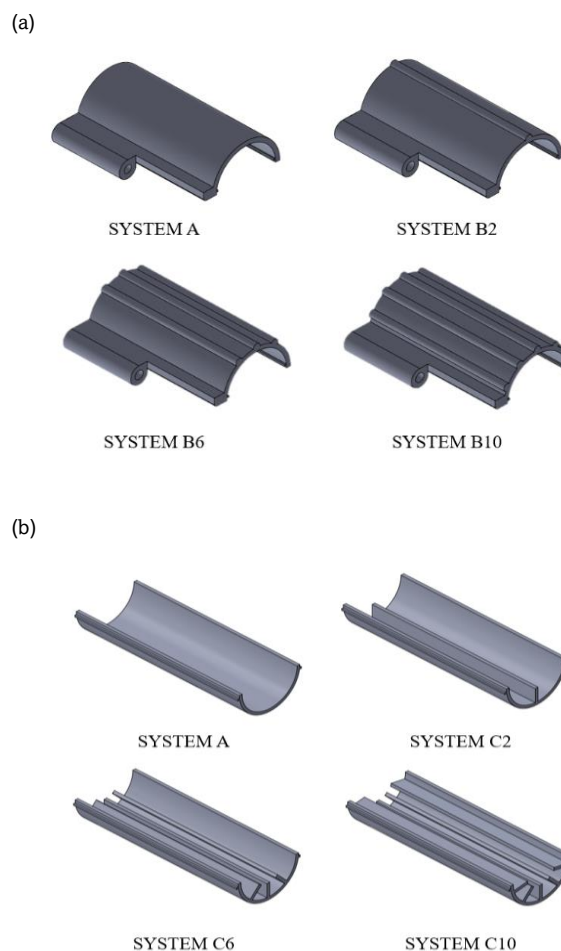


Fig 4. Surface area of the cathode for system B (a) and the anode for system C (b).

Table 3
Commercial conductive filament and their conductive composition.

Filament	Conductive Material	Composition	Reference
Polylactic Acid (PLA) Filament	Poly(3,4-ethylenedioxythiophene) coat	20% (w/v)	Chang et al., 2016
Polylactic Acid (PLA) Filament	Carbon Fiber	20% (w/w)	Bhandari et al., 2019
Polyethylene Terephthalate Glycol (PETG) Filament	Carbon Fiber	20% (w/w)	García et al., 2022
Acrylonitrile Butadiene Styrene (ABS) Plastic	Carbon Black	15% (w/w)	Jayanth et al., 2022
Thermoplastic Polyurethane (TPU) Filament	Carbon Black	30% (w/w)	Atawa et al., 2022

3. Results and Discussion

3.1 Conductive PLA as Electrode

In the study of electrochemical systems, a key component in the construction of the system to be studied is the electrode. In the context of PMFCs, electrodes should be conductive, biocompatible, chemically stable, and economical (Agrahari et al., 2022; Nidheesh et al., 2022). Carbon is an established material of choice due to its generally high conductivity, low resistance, and porous nature. Metallic electrodes in the form of stainless steel are also viable materials, except for Copper, due to their toxic effect on microbes (Maddalwar et al., 2021). In recent studies, however, the use of additive manufacturing, particularly via 3D-printing technology, has also been used for constructing conductive electrodes (Theodosiou et al., 2019). This trend, albeit still yet to be fully explored, has captured the interest of researchers in taking a new approach to PMFC studies.

Polylactic Acid (PLA), Acrylonitrile Butadiene Styrene (ABS), and Polyethylene Glycol (PETG) are among the common filaments used in 3D printing that have conductive forms which are obtained by adding a fixed amount of conductive material into the matrix, among which is carbon black (Gregory, 2022). Commercial conductive PLA is composed of 53% carbon black by mass and 26.5% by volume, with a median particle size by volume of 224 μm (Tirado-Garcia et al., 2021). Consequently, the resistivities of these filaments are higher than those of purely conductive materials such as graphite. Table 3 provides the conductive composition of commercial filaments available from literature.

In this study, conductive PLA has been used, and the obtained average resistivities for the cathode and anode of all systems measured for a 6 cm print length are 0.45 k Ω and 0.61 k Ω , respectively. In comparison, pure graphite has a resistivity of 7.35x10⁻¹³ k Ω corresponding to a similar print length (Mazloun et al., 2020). Despite this, the reproducibility of the 3D-printed materials remains an advantage over the conductivity gaps as this opens more opportunities for scale-up and power amplification.

3.2 PMFC System Performance

The plots of average voltage (mV) and average current (μA) versus time (days) for comparison of each PMFC system are provided in Figure 5 to provide a gist of the general trend of the performance. Here, all systems follow an increasing yet

dynamic trend, as evident in the varying readouts per day. There are days when the voltage and current readouts suddenly peak, while there are some when the readouts drop. This dynamic behavior of each system is accounted the uncontrollable external factors such as weather, measurement contact points, and plant health (Maddalwar et al., 2021; Nitorisavut & Regmi, 2017). The plants' phases are also hypothesized to affect the readings of each system as plants undergoing their flowering phase might retard or amplify the

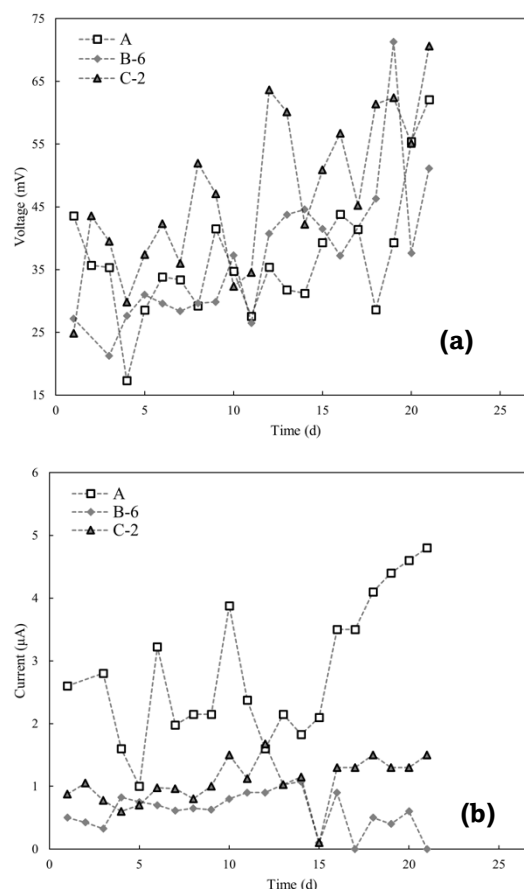


Fig 5. Daily average voltage (a) and current (b) measurements against resistances of 20 k Ω (Systems A and B-10), 24 k Ω (Systems B-2, B-6, and C-2), 50 k Ω (System C-6), and 43 k Ω (System C-10) for closed circuits of each selected system.

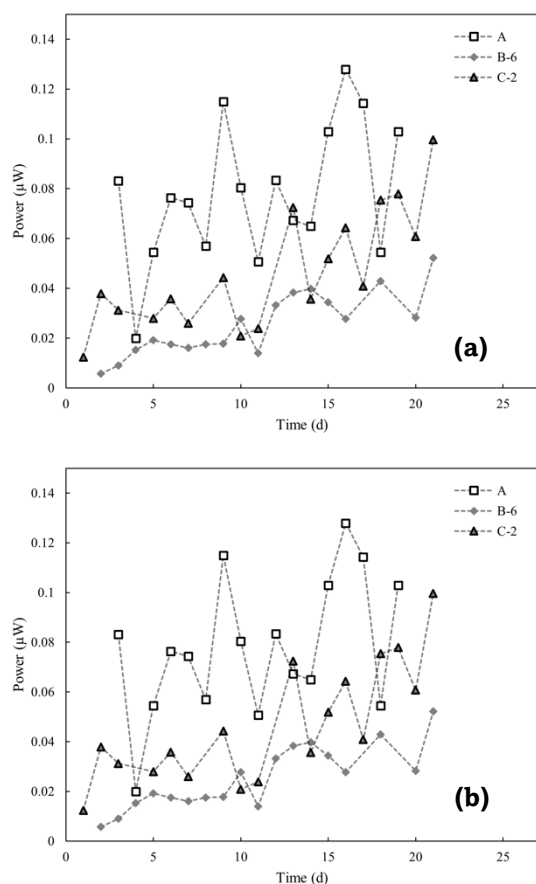


Fig 6. Daily average measurements of power (a) and power density (b) for closed circuit.

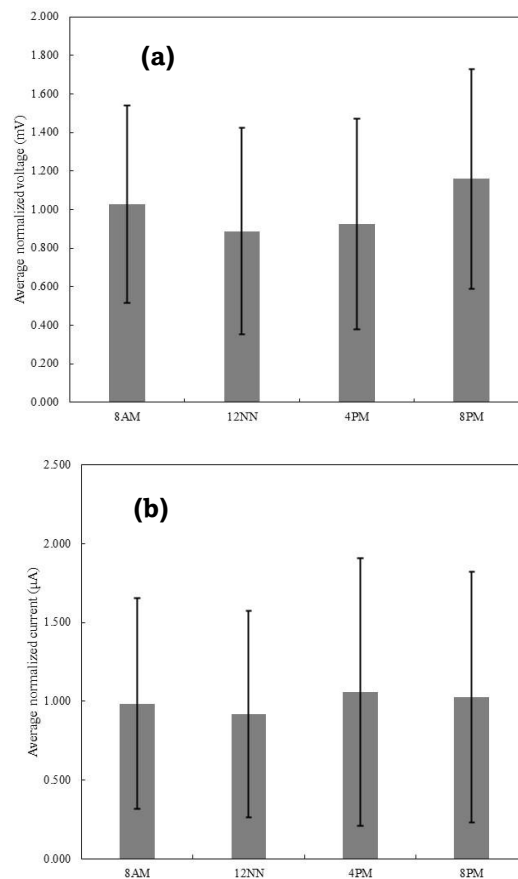


Fig 7. Average normalized voltage (a) and current (b) readings of measurement for all systems.

organic matter deposition on their roots which the electrogenic bacteria consumes. Apart from this, the voltage versus time plot also suggests that System C-2 achieves the highest voltage readouts among others, while System B-6 has the lowest variance in the readings. Essentially, the plots imply that in terms of voltage readings, System C-2 achieves the highest, while in terms of consistency, System B-6 has the best performance. To assess the response of PMFC systems relative to their measuring period, graphs of the normalized voltage (mV) and current (μA) readings are provided in Figure 7. Graphically, the figure shows that the voltage and current peak at 8 PM, thereby suggesting that the power generation of each system is at its highest at night. The average voltage measured at this time period is significantly larger compared to 12NN ($\alpha = 0.05$). This occurrence is hypothesized by the researchers as a result of a delayed release of organic substrates on the roots of the plant. From the context of biochemistry, plants' metabolic processes are generally classified into two – the light-dependent reaction (photosynthesis) and the light-independent reaction (cellular respiration) (Karakaya *et al.*, 2021). In the study performed by Begcy *et al.*, it was determined that shading is the primary factor restricting plant growth and metabolism (Begcy *et al.*, 2022). Since the PMFC systems are partially shaded, photosynthesis occurs at a lesser rate than the cellular respiration of the plant, and thus, most of its metabolic processes occur at night. Because the plants are more akin to the latter reaction, the organic substrates, which would otherwise be normally released during the day, are delayed.

3.3 Electrode Surface Area Variation

Plots of power, power density, maximum power, and maximum power density are provided in Figure 8. Here, System A is at a cathode-anode (C/A) ratio of 1.87, while ratios less than and greater than 1.87 corresponds to Systems C and B, respectively. Thus, the design benefits from increasing the cathode surface area, as illustrated by the increasing power and density trend with an increasing C/A ratio. This suggests that the PMFC is cathode-limited, and its design aspects should be focused on the cathode.

The kinetics of the electrochemical reaction occurring in the PMFC involves microbial oxidation of organic substrates to produce electrons, protons, and carbon dioxide (CO_2) and the reduction of oxygen, protons, and electrons to form water molecules (Fadzli *et al.*, 2021; Kabutey *et al.*, 2019). The rate of these half-cell reactions should be equal to sustain stable electricity generation. Considering that the design is cathode-limited, reduction, therefore, occurs at a slower rate than oxidation. Consequently, too many protons from oxidation from the anode are transported onto the cathode, which it cannot immediately process. To compensate for this drawback, a larger cathode surface area is desired to open more sites for reduction and match the rate of anode half-reaction. This parallels an existing compartmentalization study in which the results also favor an increase in anode surface area to balance the kinetics of electrochemical reaction in the cell (Pamintuan, Reyes, et al., 2020).

Figure 8 also shows that the power and power density peaks at ratios between $1.87 \text{ mm}^2/\text{mm}^2$ and $2.05 \text{ mm}^2/\text{mm}^2$. Thus, a cathode-anode surface area ratio of 2:1 is optimum for

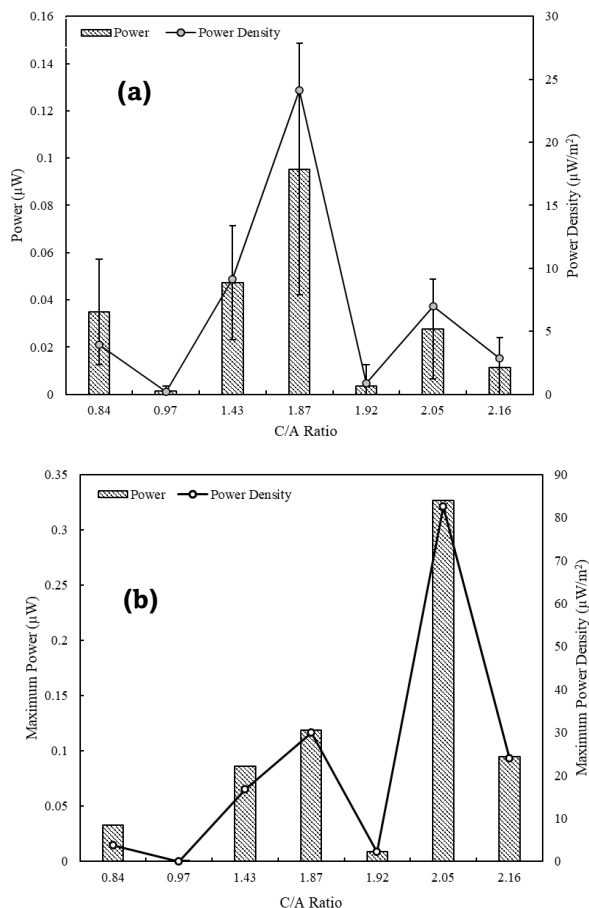


Fig 8. Effect of surface area ratio variation on the average power and power density (a) and maximum power and maximum power density (b) of the PMFC systems

this design. Beyond these ratios, additional resistance will build up and ultimately hamper the power output. The fluctuations in ratios of 0.97 mm²/mm² and 1.92 mm²/mm² are due to faulty cells and other uncontrollable factors. Likewise, the difference in peak power in terms of average voltage readings and polarization studies are accounted for the same reason. These anomalies imply that the PMFC performance is not entirely dependent on the electrode surface area alone but also on plant health and other external factors.

3.4 Effect of Plant on Power Generation

To investigate the effect of plant health on PMFC performance, the plants of the best performing (Systems A, B-6, and C-10, respectively) and least performing systems (Systems C-6, B-2, B-10, respectively) were swapped, and their corresponding voltage readings were measured according to their peak time, every day, for 5 days. The plant for System C-2 was held as is since this lies in the middle of the performance ranking. The increased readings for this system after the 5-day experiment was accounted for the continuous power generation of the system. Figure 9 shows the comparison of the voltage readings of each system after swapping the plants.

The graph implies that the voltage readings of the best-performing systems had dropped after swapping the plants with those of the least-performing systems. System B-2 had an increased voltage reading for the swapped plants based on Figure 9b, which was formerly one of the least-performing systems. Also, there is a significant difference between the

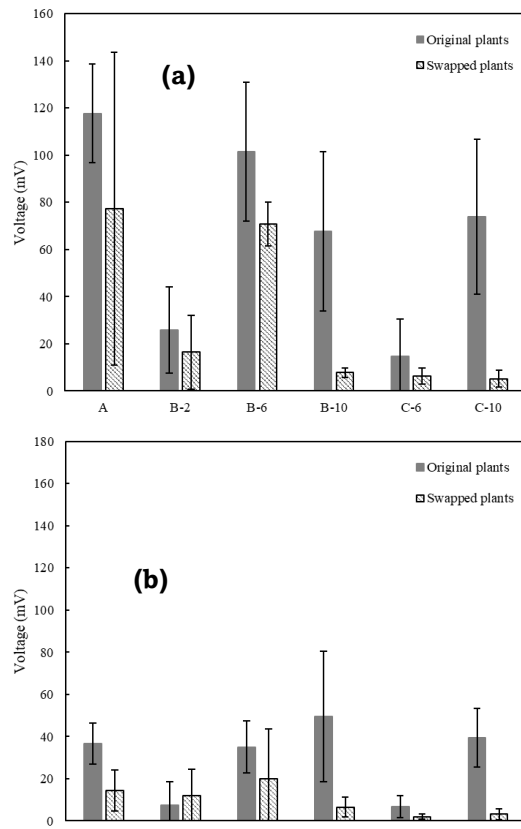


Fig 9. Comparison of the averaged daily voltage readings of systems with original plants and the swapped plants for open circuit (a) and closed circuit (b).

average voltage of swapped plants and the original plants for both the open and closed circuits ($\alpha = 0.05$). Therefore, this suggests that plant health is another contributing factor to the PMFC performance apart from the electrode surface area. Suffice it to say, the low performance of some PMFC systems is not entirely due to the design but is also attributed to plant health.

3.5 Polarization

Polarization tests were done before and after the 21-day voltage and current measurements. Resistor loads of values 100Ω to 430,000Ω were used, and the corresponding voltage readings (mV) were recorded. Figure 10 shows the plots of voltage versus resistance for all the systems involved in the study. Here, the trend of the curves is governed by Ohms law, $V=IR$, since the voltage readings can be seen to increase together with the resistance values (M. Sharma et al., 2022). The trend plateaus, however, as the system achieves its maximum voltage reading corresponding to the maximum allowable external resistance.

The optimum resistor value for each system ranges from 20,000Ω to 50,000Ω, and the average maximum power densities for systems A, B, and C are 26.99 μW/m², 36.24 μW/m², and 6.81 μW/m², respectively. This design's highest maximum power density was 82.54 μW/m², corresponding to System B-6. The high external resistance of the PMFC systems can be accounted for by the high resistivity of the 3D prints since, unlike graphite electrodes, conductive PLAs are not entirely made of conductive materials. To further improve of the novel design, a decrease in internal resistance should be one of

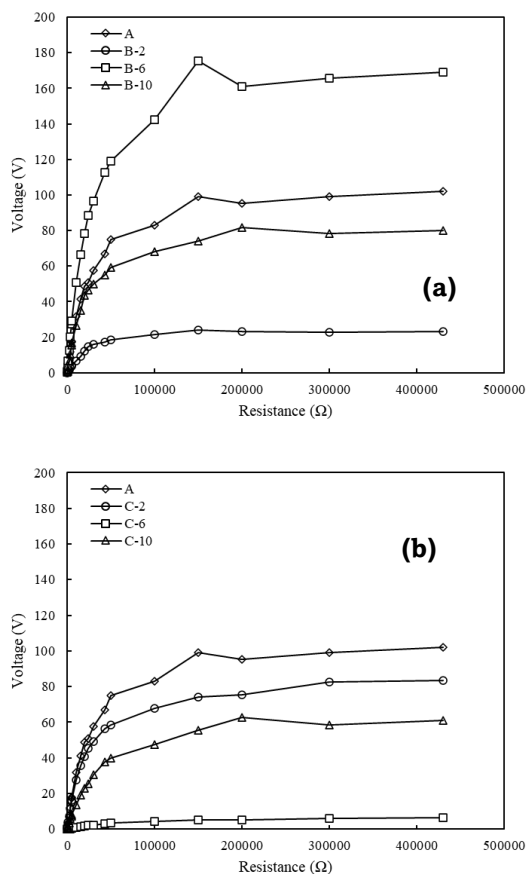


Fig 10. Response of voltage with increasing resistance load for systems with anode-limited variations (a) and cathode-limited variations (b).

the design considerations, and this can be done by utilizing an electrode material of higher conductivity or optimizing the electrode configuration.

3.6 PMFC as a hybrid of battery and generator

In conjunction with the polarization conducted in this study, graphs of voltage-current (V-I) curves were also plotted for each system. The trend of these V-I curves generally follows a decreasing trend, as illustrated in Figure 11. This is comparable to those of batteries and generators, which, on the other hand, follow a decreasing logarithmic trend (Rawa et al., 2023). This suggests that PMFCs are comparable to batteries and generators in such a way that the former generates and stores electricity. This is further supported by the voltage readings and graphs previously shown in Figure 5, wherein the PMFC systems indeed generate their own electricity, and the extended relationship between the system and the microbes suggests that it can also store its generated electricity (De La Rosa et al., 2019; Greenman et al., 2019; Y. Wang et al., 2019).

Moreover, the V-I curve in Figure 11b shows the regions of ohmic and activation losses for the PMFC. As stated in a recently concluded polarization study of an MFC, these curves are generally divided into three sections: a section of rapid voltage drop, followed by a section of linear voltage drop, and ends with another section of rapid voltage drop to which the current density is maximum (Santana et al., 2020; Simeon et al., 2020). Respectively, these regions correspond to activation, ohmic, and mass transfer losses for the system. Ohmic losses

are seen to be predominant among the other losses, and this can be accounted for the high resistivity of the 3D prints, unlike those of purely conductive materials. Nonetheless, these curves postulate the idea that PMFCs can be a hybrid between a battery and a generator, and their behavior agrees with those obtained from the literature.

3.7 Comparison with crude assemblies

As initially mentioned, the critical components of PMFC construction are the electrodes, and the materials suitable for its construction should exhibit the characteristics of conductive, biocompatible, chemically stable, and economical. This study explored the performance of a novel 3D-printed aquatic PMFC using conductive PLA electrodes. Table 4 summarizes the performance of existing PMFCs from the literature with varying electrode materials as well as the plants used.

Clearly, the performance of the designed PMFC study is not on par with those of PMFCs retrofitted with purely conductive materials. Among the listed materials, the stainless-steel mesh with activated carbon yielded the highest maximum power density. Meanwhile, the maximum average power density obtained in this study is lower than those in the literature, which is mainly accounted for the difference in electrode material used.

Based on the experimental study, the plant affects the performance of the PMFC. In the studies of Pamintuan et al. in Table 4., the maximum power densities of the same PMFC setup vary with the plant used. This is better observed in the maximum power densities yielded by PMFC setups using *Azolla pinnata* and *Lemna minor*. This occurrence also agrees with the results of this study, as evident in the varied performance of PMFCs with swapped plants. In a gist, PMFCs are complex

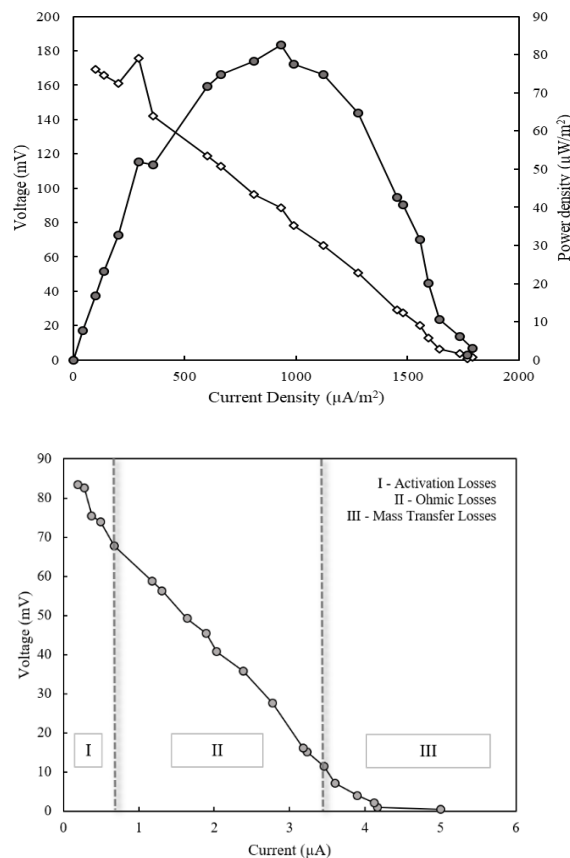


Figure 11. Polarization curves for System B-6 (a) and V-I curve for System C-2 (b).

Table 4

Bibliographic analysis of PMFC performance using different plant species and electrode materials.

Author	Plant	Description	Maximum Power Density
Fang <i>et al.</i> , 2015	<i>Ipomoea aquatica</i>	Stainless steel mesh activated carbon electrodes; single-cell PMFC	852 $\mu\text{W}/\text{m}^2$
Song <i>et al.</i> , 2017	<i>Phragmites australis</i>	Granular activated carbon electrodes; single-cell PMFC	150 $\mu\text{W}/\text{m}^2$
Author	Plant	Description	Maximum Power Density
Xu <i>et al.</i> , 2017	<i>Vallisneria spiralis L.</i>	Graphite felt electrodes; single-cell PMFC	3.16 mW/m^2
Nitorisavut & Regmi, 2017	<i>Cyperus involucratus R.</i>	Graphite felt electrodes; single-cell PMFC	5.99 mW/m^2
Oon <i>et al.</i> , 2017	<i>Elodea nuttallii</i>	Activated Carbon electrodes; single-cell PMFC	184.8 \pm mW/m^2
Wang <i>et al.</i> , 2017	<i>Canna Indica</i>	Carbon fiber felt electrode; single-cell PMFC	8.91 mW/m^2
Pamintuan <i>et al.</i> , 2018	<i>Eichhornia crassipes</i>	Graphite rod electrodes; single-cell PMFC	290 $\mu\text{W}/\text{m}^2$
Pamintuan <i>et al.</i> , 2019	<i>Azolla pinnata</i>	Woven carbon fiber electrodes; single-cell PMFC	3.43 $\mu\text{W}/\text{m}^2$
	<i>Lemna minor</i>		247.11 $\mu\text{W}/\text{m}^2$
	<i>Iris pseudacorus</i>		25.14 mW/m^2
Yang <i>et al.</i> , 2020	<i>Phragmites australis</i>	Graphite gravel electrodes; single-cell PMFC	21.70 mW/m^2
	<i>Hyacinth Pink</i>		8.74 mW/m^2
This study	<i>Eichhornia crassipes</i>	Conductive PLA electrodes; single-cell PMFC	82.54 $\mu\text{W}/\text{m}^2$

systems that are an interplay between electrode surface area and other external factors. Theoretically, electrode surface area helps PMFC performance; realistically, other factors come into play.

3.8 Future Challenges

This study explored an untapped area in the improvement of PMFC studies and aims to pave the way for future studies on aquatic systems capitalizing on 3D-printing technology. Despite its prospects, it is faced with various technological and biological limitations such as its low individual bioelectricity generation, reliance on plant health, and lack of standardized design. However, various studies have emerged from the realm of PMFC technology focusing on tackling its major bottlenecks. Some steered its direction towards integrating PMFC technology in wastewater treatment – resulting in a simultaneous power generation and pollution control (Pamintuan *et al.*, 2018). This indicates that utilizing the design as a retrofit to other technologies can compensate for its individual limitations. is mainly accounted for the difference in electrode material used.

Power amplification, design integration, and identifying the ideal model plant are among the recommended areas of focus for future endeavors in this study. Stacking efficiency studies are the best option to amplify its bioelectricity generation since this also makes use of the rapid prototyping advantage of the 3D-printed design (Pamintuan, Ancheta, *et al.*, 2020; Theodosiou *et al.*, 2019) Moreover, the lower resistance on aquatic systems contributes to the potential increase in power generation of the design. Apart from this, coupling the design with other technologies such as in wastewater treatment or aquaponic systems makes use of its potential of simultaneous power generation, which is another way to overcome its limitations. is mainly accounted for the difference in electrode material used.

In its current state, the prospect of this study outweighs its limitations. If engineered properly, the design can proceed in large-scale applications and introduce a new era of smart agriculture. This ultimately contributes to the United Nations Sustainable Development Group (UNSDG) goals for a sustainable future, specifically, on its goal of achieving sustainable and clean energy, clean water and sanitation, and climate action. The results of this study are an initial step towards this envisioned future, and devising solutions in its future challenges will gradually lead us to the sustainable future we all hope for.

4. Conclusion

This study had explored the performance of a novel aquatic PMFC with 3D-printed components. Using conductive PLA as the electrode material, a maximum power density of 82.54 $\mu\text{W}/\text{m}^2$ was achieved. As hypothesized, the design achieves lesser power than the existing PMFCs in the literature due to the fixed amount of conductive materials present in its matrix. Despite this, the rapid-prototyping advantage of 3D-printing provides benefit for stacking studies and other scale-up aspects of the design.

The variations in electrode surface area provided results suggesting that the design benefits by increasing the cathode surface area; hence the design is cathode-limited, with an optimum cathode-anode surface area ratio of 2:1. However, the performance of PMFC systems with swapped plants adds the idea that the determining factor for the design's performance is not limited to electrode surface area alone, but also to plant health. This agrees with the results obtained from the literature, as PMFCs with similar setups but different plants exhibit different power densities due to the differences in organic matter deposition dictated by plant's health.

Overall, the performance of the novel, fully submerged, 3D-printed aquatic PMFC was successfully evaluated in this study – the first of its kind. The results paved the way for the potential use of 3D printing in developing aquatic PMFCs and capitalizing on the lower internal resistance present in aquatic systems. Despite its reproducibility, the scale-up aspect was not explored in this study and, as such, is suggested for further investigation. By filling these gaps, we can hope to achieve sustainable energy by taking advantage of the existing technologies.

Acknowledgments

The researchers would like to express their gratitude to Mapua University and to the professors for making this study possible.

Author Contributions: MPDM: Conceptualization, methodology, experimentation, formal analysis, writing—original draft, HJFV; Conceptualization, methodology, experimentation, formal analysis, writing—original draft, KRSP; writing—review and editing, project administration, validation. All authors have read and agreed to the published version of the manuscript.

Funding: This research was funded by Mapua University

Conflicts of Interest: The authors declare no conflict of interest.

References

- Agrahari, R., Bayar, B., Abubakar, H. N., Giri, B. S., Rene, E. R., & Rani, R. (2022). Advances in the development of electrode materials for improving the reactor kinetics in microbial fuel cells. *Chemosphere*, *290*, 133184. <https://doi.org/10.1016/J.CHEMOSPHERE.2021.133184>
- Atawa, B., Maneval, L., Alcouffe, P., Sudre, G., David, L., Sintesz, Zydowicz, N., Beyou, E., & Serghei, A. (2022). In-situ coupled mechanical/electrical investigations on conductive TPU/CB composites: Impact of thermo-mechanically induced structural reorganizations of soft and hard TPU domains on the coupled electro-mechanical properties. *Polymer*, *256*, 125147. <https://doi.org/10.1016/J.POLYMER.2022.125147>
- Begcy, K., Wang, M., Chen, L. L., Wen, J., Qin, F., Shen, Y., Li, Z., Qu, H., Feng, J., Kong, L., Teri, G., Luan, H., & Cao, Z. (2022). *Shade Delayed Flowering Phenology and Decreased Reproductive Growth of Medicago sativa* L. *13*, 835380. <https://doi.org/10.3389/fpls.2022.835380>
- Bhandari, S., Lopez-Anido, R. A., & Gardner, D. J. (2019). Enhancing the interlayer tensile strength of 3D printed short carbon fiber reinforced PETG and PLA composites via annealing. *Additive Manufacturing*, *30*. <https://doi.org/10.1016/J.ADDMA.2019.100922>
- Chang, H. C., Sun, T., Sultana, N., Lim, M. M., Khan, T. H., & Ismail, A. F. (2016). Conductive PEDOT:PSS coated polylactide (PLA) and poly(3-hydroxybutyrate-co-3-hydroxyvalerate) (PHBV) electrospun membranes: Fabrication and characterization. *Materials Science and Engineering: C*, *61*, 396–410. <https://doi.org/10.1016/J.MSEC.2015.12.074>
- Dave, K., Darji, P., Gandhi, F., Singh, S., & Jadav, D. (2020). *Bioelectrochemical Sysytem: An Eco-Friendly Approach To Generate Electricity Utilizing Plants And Microorganisms*. <https://doi.org/10.21203/rs.3.rs-64793/v1>
- De La Rosa, E. O., Castillo, J. V., Campos, M. C., Pool, G. R. B., Nuñez, G. B., Atoche, A. C., & Aguilar, J. O. (2019). Plant Microbial Fuel Cells–Based Energy Harvester System for Self-powered IoT Applications. *Sensors (Basel, Switzerland)*, *19*(6). <https://doi.org/10.3390/S19061378>
- Fadzli, F. S., Bhawani, S. A., & Adam Mohammad, R. E. (2021). Microbial Fuel Cell: Recent Developments in Organic Substrate Use and Bacterial Electrode Interaction. *Journal of Chemistry*, *2021*. <https://doi.org/10.1155/2021/4570388>
- Fang, Z., Song, H. L., Cang, N., & Li, X. N. (2015). Electricity production from Azo dye wastewater using a microbial fuel cell coupled constructed wetland operating under different operating conditions. *Biosensors and Bioelectronics*, *68*, 135–141. <https://doi.org/10.1016/j.bios.2014.12.047>
- Garbini, G. L., Barra Caracciolo, A., & Grenni, P. (2023). Electroactive Bacteria in Natural Ecosystems and Their Applications in Microbial Fuel Cells for Bioremediation: A Review. *Microorganisms*, *11*(5), 1255. <https://doi.org/10.3390/microorganisms11051255>
- García, E., Nuñez, P. J., Caminero, M. A., Chacón, J. M., & Kamarthi, S. (2022). Effects of carbon fibre reinforcement on the geometric properties of PETG-based filament using FFF additive manufacturing. *Composites Part B: Engineering*, *235*, 109766. <https://doi.org/10.1016/J.COMPOSITESB.2022.109766>
- Greenman, J., Gajda, I., & Ieropoulos, I. (2019). Microbial fuel cells (MFC) and microalgae; Photo microbial fuel cell (PMFC) as complete recycling machines. In *Sustainable Energy and Fuels* (Vol. 3, Issue 10, pp. 2546–2560). Royal Society of Chemistry. <https://doi.org/10.1039/c9se00354a>
- Gregory, N. (2022). Measuring the Electrical Properties of 3D Printed Plastics in the W-Band. *Electrical Engineering Undergraduate Honors Theses*. <https://scholarworks.uark.edu/eleguht/85>
- Halpenny, M. (2021). *Workshop on Open-Source Microbial Fuel Cells*.
- Helder, M., Strik, D. P. B. T. B., Hamelers, H. V. M., Kuhn, A. J., Blok, C., & Buisman, C. J. N. (2010). Concurrent bio-electricity and biomass production in three Plant-Microbial Fuel Cells using *Spartina anglica*, *Arundinella anomala* and *Arundo donax*. *Bioresource Technology*, *101*(10), 3541–3547. <https://doi.org/10.1016/J.BIORTECH.2009.12.124>
- Jayanth, N., Senthil, P., & Mallikarjuna, B. (2022). Experimental investigation on the application of FDM 3D printed conductive ABS-CB composite in EMI shielding. *Radiation Physics and Chemistry*, *198*, 110263. <https://doi.org/10.1016/J.RADPHYSICHEM.2022.110263>
- Kabutey, F. T., Zhao, Q., Wei, L., Ding, J., Antwi, P., Quashie, F. K., & Wang, W. (2019). An overview of plant microbial fuel cells (PMFCs): Configurations and applications. *Renewable and Sustainable Energy Reviews*, *110*, 402–414. <https://doi.org/10.1016/j.rser.2019.05.016>
- Karakaya, F., Yilmaz, M., & Ince Aka, E. (2021). Examination of Pre-Service Science Teachers' Conceptual Perceptions and Misconceptions about Photosynthesis. *Pedagogical Research*, *6*(4), em0104. <https://doi.org/10.29333/pr/11216>
- Krishnan, S. K., Kandasamy, S., & Subbiah, K. (2021). Chapter 32 - Fabrication of microbial fuel cells with nanoelectrodes for enhanced bioenergy production. In R. P. Kumar & B. Bharathiraja (Eds.), *Nanomaterials* (pp. 677–687). Academic Press. <https://doi.org/10.1016/B978-0-12-822401-4.00003-9>
- Maddalwar, S., Kumar Nayak, K., Kumar, M., & Singh, L. (2021). Plant microbial fuel cell: Opportunities, challenges, and prospects. *Bioresource Technology*, *341*, 125772. <https://doi.org/10.1016/J.BIORTECH.2021.125772>
- Mazloun, A., Kováčik, J., Zagari, A., & Sevostianov, I. (2020). Copper-graphite composite: Shear modulus, electrical resistivity, and cross-property connections. *International Journal of Engineering Science*, *149*, 103232. <https://doi.org/10.1016/J.IJENGSCI.2020.103232>
- Nidheesh, P. V., Ganiyu, S. O., Kuppam, C., Mousset, E., Samsudeen, N., Olvera-Vargas, H., & Kumar, G. (2022). Bioelectrochemical cells as a green energy source for electrochemical treatment of water and wastewater. *Journal of Water Process Engineering*, *50*, 103232. <https://doi.org/10.1016/j.jwpe.2022.103232>
- Nitorisavut, R., & Regmi, R. (2017). Plant microbial fuel cells: A promising biosystems engineering. *Renewable and Sustainable Energy Reviews*, *76*, 81–89. <https://doi.org/10.1016/J.RSER.2017.03.064>
- Oon, Y. L., Ong, S. A., Ho, L. N., Wong, Y. S., Dahalan, F. A., Oon, Y. S., Lehl, H. K., Thung, W. E., & Nordin, N. (2017). Role of macrophyte and effect of supplementary aeration in up-flow constructed wetland-microbial fuel cell for simultaneous wastewater treatment and energy recovery. *Bioresource Technology*, *224*, 265–275. <https://doi.org/10.1016/J.BIORTECH.2016.10.079>

- Pamintuan, K. R. S., Ancheta, A. J. G., & Robles, S. M. T. (2020). Stacking efficiency of terrestrial Plant-Microbial Fuel Cells growing *Ocimum basilicum* and *Origanum vulgare*. *E3S Web of Conferences*, 181, 01004. <https://doi.org/10.1051/E3SCONF/202018101004>
- Pamintuan, K. R. S., Gonzales, A. J. S., Estefanio, B. M. M., & Bartolo, B. L. S. (2018). Simultaneous phytoremediation of Ni²⁺ and bioelectricity generation in a plant-microbial fuel cell assembly using water hyacinth (*Eichhornia crassipes*). *IOP Conference Series: Earth and Environmental Science*, 191(1). <https://doi.org/10.1088/1755-1315/191/1/012093>
- Pamintuan, K. R. S., Reyes, C. S. A., & Lat, D. K. O. (2020). Compartmentalization and polarization studies of a Plant-Microbial Fuel Cell assembly with *Cynodon dactylon*. *E3S Web of Conferences*, 181, 01007. <https://doi.org/10.1051/E3SCONF/202018101007>
- Pamintuan, K. R. S., Virata, M. M. D., & Yu, M. F. C. (2019). Simultaneous phytoremediation of Cu²⁺ and bioelectricity generation in a plant-microbial fuel cell assembly growing *Azolla pinnata* and *Lemna minor*. *IOP Conference Series: Earth and Environmental Science*, 344(1). <https://doi.org/10.1088/1755-1315/344/1/012021>
- Rawa, M., Al-Turki, Y., Sindi, H., Čalasan, M., Ali, Z. M., & Abdel Aleem, S. H. E. (2023). Current-voltage curves of planar heterojunction perovskite solar cells – Novel expressions based on Lambert W function and Special Trans Function Theory. *Journal of Advanced Research*, 44, 91–108. <https://doi.org/10.1016/j.jare.2022.03.017>
- Roy, H., Rahman, T. U., Tasnim, N., Arju, J., Rafid, Md. M., Islam, Md. R., Pervez, Md. N., Cai, Y., Naddeo, V., & Islam, Md. S. (2023). Microbial Fuel Cell Construction Features and Application for Sustainable Wastewater Treatment. *Membranes*, 13(5), 490. <https://doi.org/10.3390/membranes13050490>
- Santana, J., Espinoza-Andaluz, M., Li, T., & Andersson, M. (2020). A Detailed Analysis of Internal Resistance of a PEFC Comparing High and Low Humidification of the Reactant Gases. *Frontiers in Energy Research*, 8, 217. <https://doi.org/10.3389/FENRG.2020.00217/BIBTEX>
- Sharma, A., & Chhabra, M. (2021). Performance evaluation of a photosynthetic microbial fuel cell (PMFC) using *Chlamydomonas reinhardtii* at cathode. *Bioresource Technology*, 338. <https://doi.org/10.1016/J.BIORTECH.2021.125499>
- Sharma, M., Das, P. P., Sood, T., Chakraborty, A., & Purkait, M. K. (2022). Reduced graphene oxide incorporated polyvinylidene fluoride/cellulose acetate proton exchange membrane for energy extraction using microbial fuel cells. *Journal of Electroanalytical Chemistry*, 907. <https://doi.org/10.1016/j.jelechem.2021.115890>
- Simeon, M. I., Asairo, F. U., Aliyu, M., Raji, O. A., & Freitag, R. (2020). Polarization and power density trends of a soil-based microbial fuel cell treated with human urine. *International Journal of Energy Research*, 44(7), 5968–5976. <https://doi.org/10.1002/er.5391>
- Song, H., Zhang, S., Long, X., Yang, X., Li, H., & Xiang, W. (2017). Optimization of bioelectricity generation in constructed wetland-coupled microbial fuel cell systems. *Water (Switzerland)*, 9(3). <https://doi.org/10.3390/w9030185>
- Theodosiou, P., Greenman, J., & Ieropoulos, I. (2019). Towards monolithically printed Mfcs: Development of a 3d-printable membrane electrode assembly (mea). *International Journal of Hydrogen Energy*, 44(9), 4450–4462. <https://doi.org/10.1016/J.IJHYDENE.2018.12.163>
- Tirado-Garcia, I., Garcia-Gonzalez, D., Garzon-Hernandez, S., Rusinek, A., Robles, G., Martinez-Tarifa, J. M., & Arias, A. (2021). Conductive 3D printed PLA composites: On the interplay of mechanical, electrical and thermal behaviours. *Composite Structures*, 265. <https://doi.org/10.1016/J.COMPSTRUCT.2021.113744>
- Tornheim, A., & O'Hanlon, D. C. (2020). What do Coulombic Efficiency and Capacity Retention Truly Measure? A Deep Dive into Cyclable Lithium Inventory, Limitation Type, and Redox Side Reactions. *Journal of The Electrochemical Society*, 167(11), 110520. <https://doi.org/10.1149/1945-7111/AB9EE8>
- Wang, J., Song, X., Wang, Y., Bai, J., Bai, H., Yan, D., Cao, Y., Li, Y., Yu, Z., & Dong, G. (2017). Bioelectricity generation, contaminant removal and bacterial community distribution as affected by substrate material size and aquatic macrophyte in constructed wetland-microbial fuel cell. *Bioresource Technology*, 245, 372–378. <https://doi.org/10.1016/J.BIORTECH.2017.08.191>
- Wang, Y., Chen, Y., Wen, Q., Zheng, H., Xu, H., & Qi, L. (2019). Electricity generation, energy storage, and microbial-community analysis in microbial fuel cells with multilayer capacitive anodes. *Energy*, 189. <https://doi.org/10.1016/j.energy.2019.116342>
- Xu, P., Xiao, E. R., Xu, D., Zhou, Y., He, F., Liu, B. Y., Zeng, L., & Wu, Z. Bin. (2017). Internal nitrogen removal from sediments by the hybrid system of microbial fuel cells and submerged aquatic plants. *PLOS ONE*, 12(2), e0172757. <https://doi.org/10.1371/JOURNAL.PONE.0172757>
- Yang, Y., Zhao, Y., Tang, C., Xu, L., Morgan, D., & Liu, R. (2020). Role of macrophyte species in constructed wetland-microbial fuel cell for simultaneous wastewater treatment and bioenergy generation. *Chemical Engineering Journal*, 392. <https://doi.org/10.1016/J.CEJ.2019.123708>

